Product-Induced Distortion of a Metalloporphyrin Host: Implications for Acceleration of Diels−Alder Reactions

Moshe Nakash,[†] Zöe Clyde-Watson,[†] Neil Feeder,[†] John E. Davies,[†] Simon J. Teat,[‡] and Jeremy K. M. Sanders*,[†]

Contribution from the Cambridge Centre for Molecular Recognition, University Chemical Laboratory, University of Cambridge, Lensfield Road, Cambridge CB2 1EW, UK, and CLRC Daresbury Laboratory, Daresbury, Warrington WA4 4AD, UK

Received June 28, 1999

Abstract: New cyclic metalloporphyrin hosts, **6** and **7**, have been prepared. At 0.33 mM in dichloromethane at 25 °C, they accelerate 65-fold and 840-fold respectively the reaction of diene **1** and dienophile **2** and also bind the hetero Diels−Alder product **3** very strongly. More importantly, small single crystals of solvated **6**, **7**, and the **6**·**3** complex were grown and their structures were determined. As the Diels−Alder product resembles the Diels−Alder transition state, the structures of the product-free host **6** and the **6**·**3** host−product complex allow, for the first time for synthetic receptors, a detailed structural analysis of the geometrical changes imposed on an accelerating agent on binding of a Diels−Alder product. Comparison of these structures reveals that when the Diels−Alder product **3** is bound within the cavity, it induces significant structural changes in **6**. This provides the first crystallographic structural evidence that accelerated product formation can be accompanied by substantial host distortion. Desolvation of host and guests emerges as another factor, implying that solvent stabilization is not as significant for the host-accelerated reaction as in the control (host free) reaction.

Introduction

Supramolecular chemistry offers the prospect that bimolecular reactions of guests can be efficiently accelerated or catalyzed within a host cavity, but progress to date has been slow. In part this is due to the lack of information on the host's structural changes resulting from guest binding and reaction.[1] The Diels−Alder reaction is a bimolecular process that proceeds through a transition state that resembles the Diels−Alder product,[2] so achieving turnover is a challenge for biology and the synthetic chemist alike.[3] The acceleration and catalysis of Diels−Alder reactions by artificial receptors,[4,5,6] antibodies,[7] and RNA[8] is well documented but we are not aware of any crystal structures of synthetic hosts that could shed useful light on the features responsible for success or failure.[9] It is a common view that host rigidity and preorganization are paramount, but kinetic and binding results for Diels−Alder reactions accelerated by oligoporphyrins suggest that flexibility is important: host responsiveness to the geometrical demands of the guests and transition state is a key factor controlling rate and regioselectivity.[4]

The regiospecific hetero-Diels−Alder reaction of 4-pyridyl butadiene **1** with 3-nitroso pyridine **2** to give oxazine **3** (Figure 1a) can be accelerated by various metalloporphyrin trimers, such as **4** and **5** (Figure 1b), leading to a rate acceleration of 300−

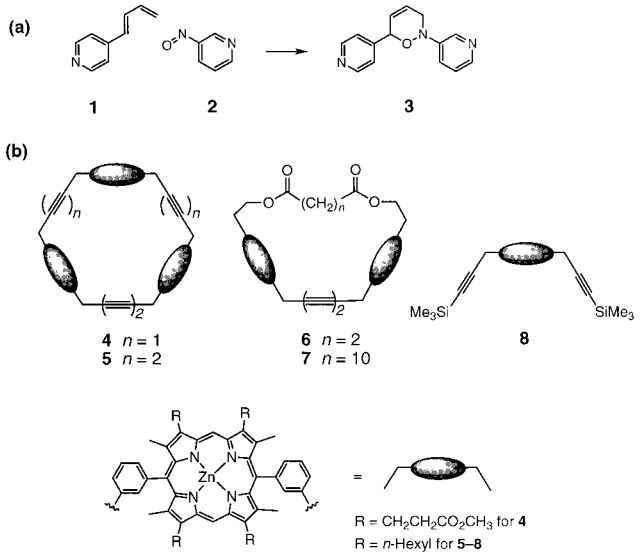

Figure 1. (a) Hetero-Diels−Alder reaction of **1** and **2** to give adduct **3**. (b) Structure of porphyrins employed in this work. Synthetic details for **4**,[4] **5**,[4] **7**,[10] and **8**[4] have been given previously.

[†] University of Cambridge.
[‡] CLRC Daresbury Laboratory.

(1) (a) Kirby, A. J. *Angew. Chem., Int. Ed. Engl.* **1996**, *35*, 707. (b) Sanders, J. K. M. *Chem. Eur. J.* **1998**, *4*, 1378.
(2) (a) Sauer, J. *Angew. Chem., Int. Ed. Engl.* **1967**, *6*, 16. (b) Houk, K. N.; Brown, F. K. *Tetrahedron Lett.* **1984**, *25*, 4609.
(3) This may be why there is only one current candidate for a natural Diels−Alderase enzyme: (a) Oikawa, H.; Katayama, K.; Suzuki, Y.; Ichihara, A. *Chem. Commun.* **1995**, 1321. (b) Oikawa, H.; Kobayashi, T.; Katayama, K.; Suzuki, Y.; Ichihara, A. *J. Org. Chem.* **1998**, *63*, 8748.
(4) Clyde-Watson, Z.; Vidal-Ferran, A.; Twyman, L. J.; Walter, C. J.; McCallien, D. W. J.; Fanni, S.; Bampos, N.; Wylie, R. S.; Sanders, J. K. M. *New J. Chem.* **1998**, *22*, 493.
(5) Marty, M.; Clyde-Watson, Z.; Twyman, L. J.; Nakash, M.; Sanders, J. K. M. *Chem. Commun.* **1998**, 2265.
(6) (a) Wang, B.; Sutherland, I. O. *J. Chem. Soc., Chem. Commun.* **1997**, 1495. (b) Rebek, J., Jr.; Kang, J. *Nature* **1997**, *385*, 50. (c) Kang, J.; Santamaria, J.; Hilmersson, G.; Rebek, J., Jr. *J. Am. Chem. Soc.* **1998**, *120*, 7389. (d) Ooi, T.; Kondo, Y.; Maruoka, K. *Angew. Chem., Int. Ed. Engl.* **1998**, *37*, 3039.
(7) (a) Meekel, A. A. P.; Resmini, M.; Pandit, U. K. *J. Chem. Soc., Chem. Commun.* **1995**, 571. (b) Hilvert, D.; Hill, K. W.; Nared, K. D.; Auditor, M.-T M. *J. Am. Chem. Soc.* **1989**, *111*, 9261. (c) Schultz, P. G.; Braisted, A. C. *J. Am. Chem. Soc.* **1990**, *112*, 7430. (d) Gouverneur, V. E.; Houk, K. N.; Pascual-Teresa, B. d.; Beno, B.; Janda, K. D.; Lerner, R. A. *Science* **1993**, *262*, 204. (e) Yli-Kauhaluoma, J. T.; Ashley, J. A.; Lo, C.-H.; Tucker, L.; Wolfe, M. M.; Janda, K. D. *J. Am. Chem. Soc.* **1995**, *117*, 7041.
(8) (a) Tarasow, T. M.; Tarasow, S. L.; Tu, C.; Kellogg, E.; Eaton, B. E. *J. Am. Chem. Soc.* **1999**, *121*, 3614. (b) Seelig, B.; Jäschke, A. *Chem. Biol.* **1999**, *6* 167.

10.1021/ja9922227 CCC: $19.00
Published on Web 05/20/2000

Table 1. Host Accelerated Rates for Formation of **3** and Binding Constant of **3** with Various Hosts, Measured in Dichloromethane at 25 °C

porphyrin host	rate acceleration[a,b] (approx.)	binding constant[c] M^{-1}
2 equiv of **8**[d]	2	6.9×10^3
4[d]	1030[e]	2.3×10^{8}[e]
5[d]	280[e]	7.3×10^{6}[e]
6	65[e]	5.6×10^{7}[e]
7	840[e]	7.1×10^{7}[e]

[a] Increase in initial rate due to the presence of 1 equiv of host molecule. [b] The measured rate constant for the control (host free) reaction is 0.0039 M^{-1} s^{-1}.[5] [c] The binding constant of oxazine **3** to the trimers corresponds to the initial bidentate interaction of the ligand with the host observed at low oxazine concentrations. [d] See ref 5. [e] To allow comparison with hosts **6** and **7** one has to consider that trimers **4** and **5** have six constructive binding possibilities for the diene + dienophile or for oxazine **3**, whereas the hosts **6** and **7** have only two constructive binding possibilities. Therefore, a trimer should inherently be 6/2 = 3 times better at accelerating the reaction and binding oxazine **3** than a host molecule that has only two Zn binding sites (as in **6** and **7**), and to compare the efficiency of the above host molecules, per two Zn binding sites, the acceleration rates and binding constants of hosts **6** and **7** should be multiplied by this factor.

1000 (Table 1).[5] We have now prepared[10] a series of capped dimers, including **6** and **7** (Figure 1b), which accelerate 65-fold and 840-fold respectively the reaction of **1** and **2** and also bind the product **3** very strongly (Table 1). Addition of 2 equiv of monomer **8** (Figure 1b) to a reaction mixture of **1** and **2** leads to an acceleration rate of only 2-fold (Table 1). This suggests that it is mainly the cyclic structures of hosts **4**−**7**, which hold the two reactants in close proximity inside the cavity, that lead to the significant acceleration rates observed with these hosts.[11] More importantly, we have succeeded in X-ray structure determinations of single crystals of methanol-solvated **6** (Figure 2), toluene/methanol-solvated **6** (Figure 3a,b), methanol-solvated **7** (Figure 4), and the **6·3** complex (Figure 3c,d). These structures provide the first crystallographic evidence that indeed accelerated product formation can be accompanied by substantial host distortion. As the Diels−Alder product resembles the Diels−Alder transition state,[2] the structures of the solvated product−free host **6** and the **6·3** host−product complex provide insight into the features responsible for Diels−Alder acceleration by metalloporphyrin hosts; desolvation of host and guests emerges as another factor.

(9) The X-ray crystal structures for complexes between an antibody and a transition state analogue and an inhibitor have been recently reported. (a) Romesberg, F. E.; Spiller, B.; Schultz, P. G.; Stevens, R. C. *Science* **1998**, *279*, 1929. (b) Heine, A.; Stura, E. A.; Yli-Kauhaluoma, J. T.; Gao, C.; Deng, Q.; Beno, B. R.; Houk, K. N.; Janda, K. D.; Wilson, I. A. *Science* **1998**, *279*, 1934.

(10) The general route is described in: Twyman, L. J.; Sanders, J. K. M. *Tetrahedron Lett.* **1999**, *40*, 6681.

(11) (a) The very weak acceleration rate observed with monomer **8** and the fact that addition of 1 equiv of product **3** to the reaction mixture of **1** and **2** in the presence of **5** strongly inhibit the reaction rate (the acceleration rate is reduced by 20-fold)[5] suggest that the accelerated reaction in the presence of such cyclic-metalloporphyrin hosts occurs inside the cavity of the host. (b) Free metal cations have also been used to accelerate Diels−Alder reactions (for recent reviews see: Kagan, H. B.; Riant, O. *Chem. Rev.* **1992**, *92*, 1007. Pindur, U.; Lutz, G.; Otto, C. *Chem. Rev.* **1993**, *93*, 741). However, as the Zn atoms in our systems are coordinated to the pyrrole rings in the porphyrin units, this is expected to reduce the positive charge on the Zn atoms and therefore to reduce their Lewis acidity, in comparison with free Zn^{2+} cations. Indeed, the charge on the Zn atom in a Zn-porphyrin unit was calculated to be only +0.4, see: Zerner, M.; Gouterman, M. *Theor. Chim. Acta* **1966**, *4*, 44. Therefore, this is expected to reduce the stabilization due to acid−base interaction between the pyridine groups and the Zn atoms in our systems, relative to such a stabilization with free Zn^{2+} cations, and could account for the low acceleration rate (of only 2-fold) observed with monomer **8**. (c) As each of the porphyrin units in hosts **4**−**7** can bind the reactants inside or outside the cavity, only a small fraction of bound host is the reactive complex (host + the two reactants *inside* the cavity) which leads to accelerated product formation. Therefore, the acceleration rates shown in Table 1 underestimate the true ability of such hosts to accelerate the Diels−Alder reaction *inside* the cavity of the host. The kinetic and stoichiometric aspects of the Diels−Alder reaction in the presence of cyclic-metalloporphyrin hosts have been thoroughly discussed elsewhere: Wylie, R. S.; Sanders, J. K. M. *Tetrahedron* **1995**, *51*, 513.

Results and Discussion

Hosts **6** and **7** were synthesized as shown in Scheme 1. Coupling the porphyrin monomer **9** to succinyl chloride or to dodecanedioyl dichloride yielded the linear species **10** and **11**, respectively; deprotection and Glaser cyclization gave **6** and **7** in overall yield of 39% and 56%, respectively. All the host accelerated reactions were carried out using 0.33 mM guests and host; methods for analysis of kinetics and binding were as described previously.[5] Small crystals of **6**, **7**, and the **6·3** complex were grown and the structures were determined.

Scheme 1. Synthetic Route to Macrocycles **6** and **7**

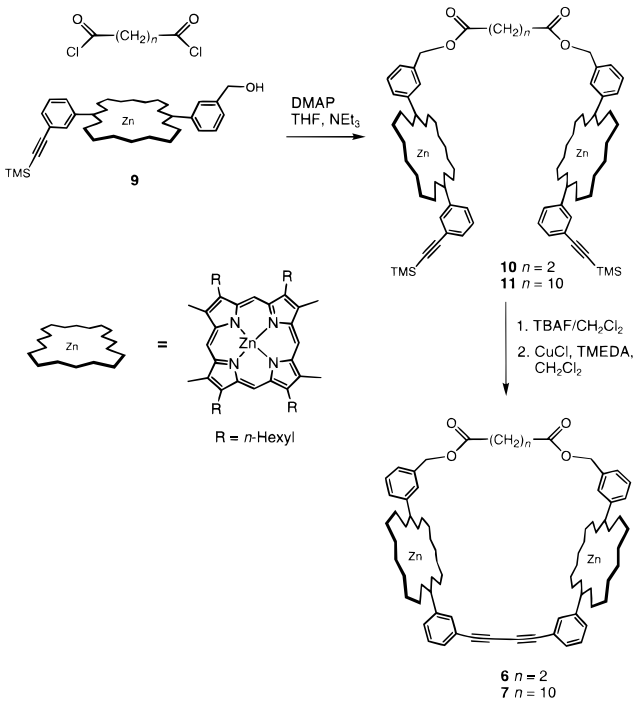

Two types of solvated **6** crystals could be grown from different solvent mixtures. From a dichloromethane/hexane/methanol mixture **6** crystallizes as a methanol-solvate in the monoclinic space group $P2_1/c$, in which two crystallographically inequivalent cyclic hosts are found in the asymmetric unit (Figure 2). From a toluene/methanol mixture, **6** crystallizes as a toluene/methanol-solvate, which has only one host in the asymmetric unit and in the orthorhombic space group *Pbca* (Figure 3a,b). In both solvated forms of **6** (Figures 2 and 3a,b) and also in the crystal structure of the **6·3** complex (Figure 3c,d), the hexyl chains (not shown) are arranged such that they block the "open" side of the cavity. In the crystal structure of **6** the two porphyrin moieties are rotated by 7.4°, 3.6°, and 6.8° with respect to each other (see Figures 2b, 2d, and 3b, respectively), indicating that the chainlike linkage is somewhat flexible, but this rotation is insignificant in the **6·3** complex (see Figure 3d). Two methanol molecules are bound to the zinc atoms within the cavity of **6**. In addition, six or eight methanol molecules are trapped in the cavity of **6** (see Figure 2a,b or Figure 2c,d, respectively,) and two toluene molecules are trapped in the cavity of **6** (see Figure 3a,b). This is in contrast to the crystal

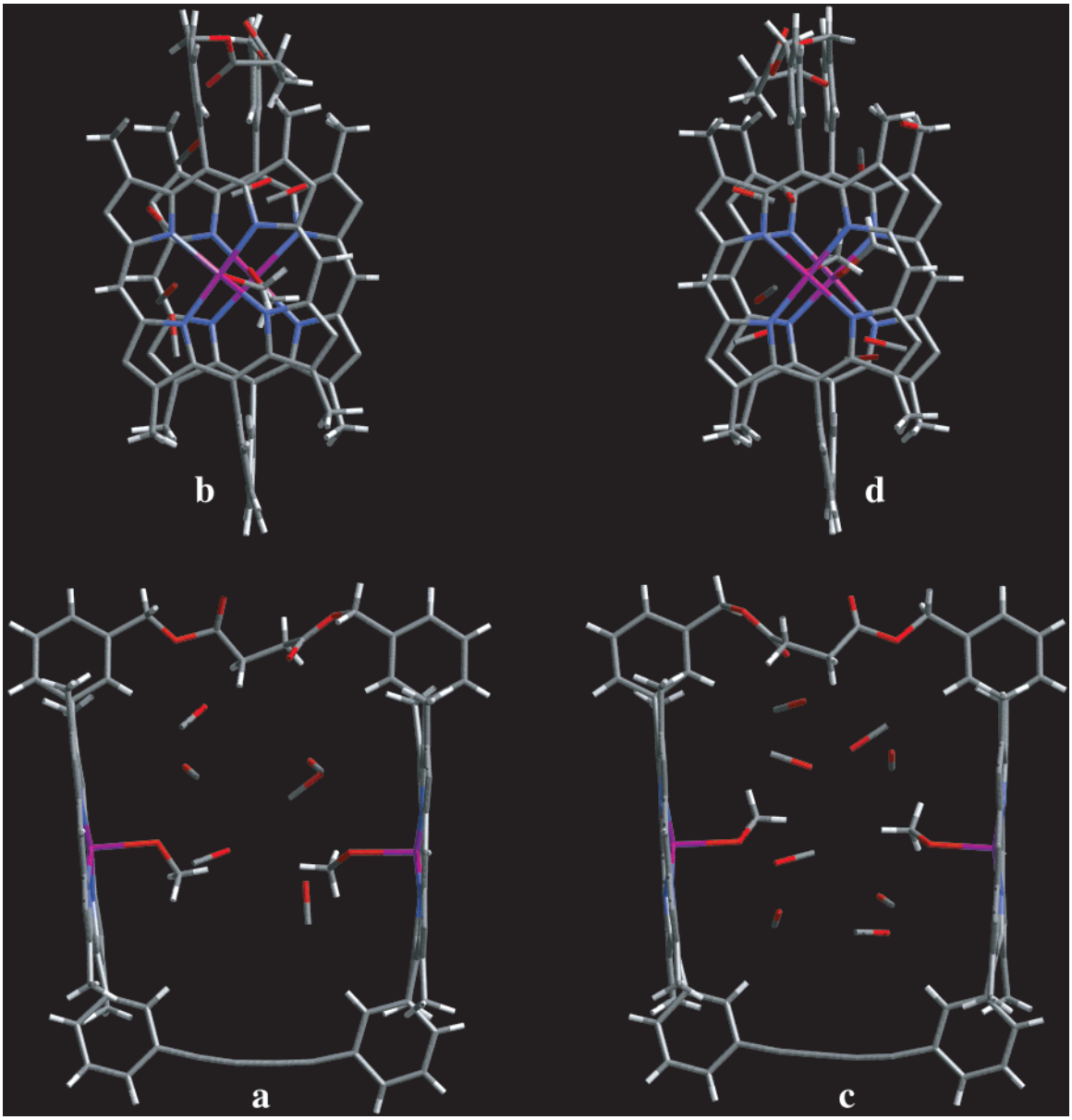

Figure 2. Two views, a and b (left host) and c and d (right host), of the crystal structure of the "free" cyclic metalloporphyrin host **6**, which contains two inequivalent macrocycles **6** (left side and right side) in the unit cell. Two MeOH molecules are bound to the Zn atoms in the host, which also contains six or eight MeOH molecules, left or right host, respectively, that are trapped in the cavity. In this crystal, the included methanol solvent molecules within the cavity of **6** exhibited considerable disorder and therefore the hydrogen atoms for these molecules are not shown. The hexyl side chains (four per porphyrin unit) have been omitted for clarity. Selected key geometrical features for **6**: Zn−Zn distance = 10.792(3) Å (left host) and = 10.828(3) Å (right host); the two Zn atoms lie at a mean distance of 0.19−0.22 Å above the N_4 plane [which are nearly coplanar, maximum deviation 0.064 Å] toward the oxygen atom; relative rotation of porphyrins = 7.4° (left host) and = 3.6° (right host); Zn−O bond lengths = 2.22(1), 2.20(1) Å (left host) and 2.21(1), 2.18(1) Å (right host).

structure of the **6·3** complex (Figure 3c,d) which does not appear to contain solvent molecules.[12a] These solvent molecules are displaced from the cavity on binding of the Diels−Alder substrates or transition state, and are absent from the product complex (as seen graphically in Figure 3). This could imply the following two effects: (a) As the Diels−Alder product is poorly solvated (if at all) inside the cavity of host **6**,[12a,b] the host-accelerated reaction is less solvated (if at all) inside the cavity of the host molecule, suggesting that solvent stabilization is not as significant for the host-accelerated reaction as in the solvated control (host free) reaction. This conclusion was reached previously from solvent effect experiments and binding results, which showed that the control reaction is faster in CH_2Cl_2 than in toluene while the host-accelerated reaction is faster in toluene than in CH_2Cl_2.[5] (b) As more than one molecule of solvent is likely to be displaced from within the cavity of host **6**, upon binding of only one ligand **3** (as seen by comparing Figures 2 or 3a with Figure 3c),[12] it is possible that the large entropic penalty expected for binding a bidentate ligand such as **3** is partially compensated by entropic gain due to solvent displacement from within the cavity. While it is in a sense obvious that some desolvation of hosts and guests is a prerequisite

(12) (a) Because of the poor quality of the diffraction data, it cannot be proved unequivocally that disordered solvent is not present in the crystal structure of the **6·3** complex. (b) However, as **3** occupies a substantial part of the cavity of **6**, clearly seen in Figure 3c and more so in the space−filling model of the **6·3** complex (not shown), the Diels−Alder product **3** is poorly solvated (if at all) inside the cavity of **6**. (c) In addition, it is likely that even if solvent is trapped in the space left in this cavity there will still be fewer molecules of solvent + ligand **3** in the cavity in the case of the **6·3** complex (Figure 3c) than in the cavity of the free host **6** (see Figures 2 and 3a).

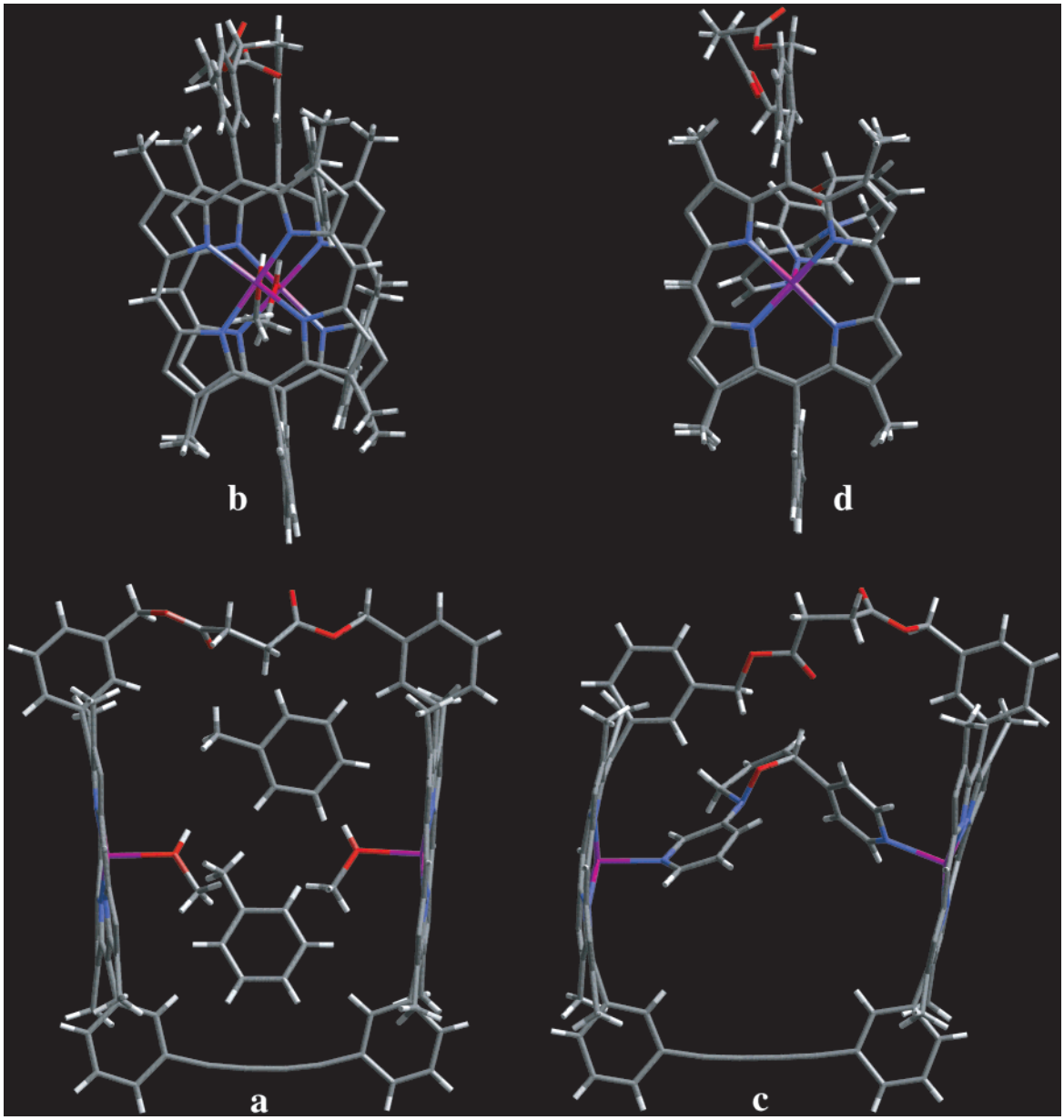

Figure 3. Two views, a and b (left side) and c and d (right side), of the crystal structures of (on the left side) the "free" cyclic metalloporphyrin host **6**, containing also two molecules of methanol and two toluene molecules, and of (on the right side) the complex between **6** and the hetero-Diels−Alder product **3**. The hexyl side chains (four per porphyrin unit) have been omitted for clarity. Selected key geometrical features for **6**: Zn−Zn distance = 10.576(5) Å; the two Zn atoms lie at a mean distance of 0.19 Å above the N_4 plane [which are nearly coplanar, maximum deviation 0.001 (left ring) and 0.064 Å (right ring)] toward the oxygen atom; relative rotation of porphyrins = 6.8°; Zn−O bond lengths = 2.20(1) and 2.28(2) Å. Selected key geometrical features for the **6·3** complex: Zn−Zn distance = 11.684(3) Å; the two Zn atoms lie at a mean distance of 0.25 (left ring) and 0.30 Å (right ring) above the N_4 planes [which are nearly coplanar, maximum deviation 0.008 (left ring) and 0.019 Å (right ring)] toward the pyridine nitrogen atom; relative rotation of porphyrins = 0.1°; N_{Py}−N_{Py} distance = 7.52(3) Å; Zn−N_{Py} = 2.20(2) Å (left porphyrin unit), Zn−N_{Py} = 2.18(2) Å (right porphyrin unit).

for the chemistry to occur, it is rare to see such a graphic demonstration of solvent displacement by a ligand guest molecule.[13]

The solvated structures of **6** (Figures 2 and 3a,b) have the same qualitative rectangular structure, in which the two porphyrin moieties are virtually planar and almost parallel and have similar Zn−Zn distances. We chose the toluene solvated structure (Figure 3a,b) for detailed structural comparison with the **6·3** complex (see below); obviously, comparison of the **6·3** complex with the structures in Figure 2 would lead to the same qualitative conclusions. As the crystal structure of **6** (Figure 3a,b) does not contain a bidentate ligand that could induce significant structural distortion, we will refer to it as the free host **6**. The **6·3** complex (Figure 3c,d) crystallizes from a dichloromethane/hexane/methanol mixture in the centrosymmetric monoclinic space group $P2_1/n$, with a racemic pair of enantiomeric oxazine molecules within the structure. The N−N distance between the two pyridine nitrogens in the bound oxazine **3** is 7.52(3) Å. **3** is a viscous oil, and attempts to obtain crystals for an unbound oxazine **3** from different combinations of solvents and temperatures were unsuccessful. Force field calculations for **3** show that the calculated oxazine ring has a similar structure to that found in the **6·3** complex but that the two pyridine rings are rotated to a different extent (23° and 35°

(13) In some systems, displacement of solvent molecules has been suggested as the driving force for binding and acceleration: (a) Kang, J.; Rebek, J., Jr. *Nature* **1996**, *382*, 239. (b) See also ref 6c.

for the 3-pyridine ring and for the 4-pyridine ring, respectively) with respect to the oxazine ring.[14] This leads to a calculated N−N distance between the two pyridine nitrogens in **3** of 8.1 Å, some 0.6 Å larger than found in the crystal. The Zn−N intermolecular distances between the two zinc atoms and the 3-pyridine and the 4-pyridine nitrogens in the **6·3** complex are 2.20(2) and 2.18(2) Å, respectively; these are consistent with other zinc porphyrin−pyridine complexes.[15]

The dihedral angles between the pyridine ring plane and the N_4 plane are 61.7(5)° and 59.0(6)° for the 3-pyridine and the 4-pyridine, respectively. These features are unusual for monomeric pyridine·zinc porphyrin complexes, where the pyridine ring is normally almost perpendicular to the porphyrin ring,[15] but do appear to be characteristic of oligomers that contain pyridylporphyrin−metalloporphyrin linkages.[16] In the latter cases, the lack of orthogonality has been rationalized by crystal packing effects, but this explanation is not tenable in the **6·3** complex where the distortion is an inevitable result of the geometrical mismatch between host and guest (see below). The tilted position of the pyridine rings in the **6·3** complex implies that the presumed perpendicular binding of the two substrates does not lead directly to the transition state geometry.

Comparison of the solvated structure of the free host **6** (Figure 3a) with that of the **6·3** complex (Figure 3c) reveals that when the Diels−Alder product **3** is bound within the cavity, it induces structural changes in **6**: the two porphyrin moieties are pushed apart, increasing the Zn−Zn distance by 1.1 Å (see Figure 3); the right-hand porphyrin is forced to lean away from the cavity while remaining virtually planar; and the left-hand porphyrin adopts a strikingly domed shape and a slight lean toward the cavity. The degree of leaning toward or away from the cavity (of the porphyrin units) can be estimated by the angle between three meso porphyrin carbons, of which two are connected to the butadiyne linker and one is connected to the diester linker.[17a] For the left-hand porphyrin unit in the **6·3** complex (Figure 3c) this angle is 86°, indicating that this porphyrin unit leans slightly toward the cavity, while for the right-hand porphyrin unit in the **6·3** complex this angle is 103°, indicating that this porphyrin unit leans away from the cavity. For comparison, these angles for both porphyrin units in the qualitatively rectangular molecular structure of **6** (Figure 3a) are 94°. These changes result from the orientation of the pyridine rings and lone pairs in **3** relative to the Zn sites in **6**. In particular, the N_{py}−Zn−Zn angles are 5.2(6)° and 21.3(4)° for the 3- and 4-pyridine, respectively. These structural changes to accommodate the product **3** are facilitated by the flexible diester chain linkage, which is significantly stretched in the product complex. The ability of host **6** to change its structure is responsible for the observation that it binds **3** very strongly and is able to accelerate the reaction of **1** and **2** (see Table 1), although the Zn−Zn distance in the free host **6** (10.576(5) Å, Figure 3a) is much shorter than that in the **6·3** complex (11.684(3) Å, Figure 3c), and even more so in the transition state complex (in which this distance is expected to be ∼13.5 Å, see below). Therefore, if **6** would not be able to distort its structure as seen in Figure 3, it would be less effective in stabilizing the transition state complex and in accelerating the reaction in Figure 1a. Obviously, host molecules with a longer Zn−Zn distance, closer to that expected in the transition state complex, should have better potential in accelerating the reaction in Figure 1a. There are other examples where flexibility has also been invoked as a key feature of catalytic success.[1b,18]

Although the two crystal structures of **6** (Figures 2 and 3a,b) have quite different packing and cavity solvation, they retain the same qualitative rectangular structure, in which the two porphyrin moieties are virtually planar and almost parallel and have similar Zn−Zn distances (see above). This implies that for the **6·3** complex (Figure 3c,d) we are observing fundamental structural changes rather than purely environmental effects.

The bicyclo[2.2.2.]octene system, such as **12**, is commonly regarded as a transition state analogue for the Diels−Alder reaction.[7a−d,9] The ethano bridge in such systems locks the cyclohexene ring (or the oxazine ring in **12**) in a conformation that resembles the proposed pericyclic transition state[2] for the Diels−Alder reaction of a cisoid diene and dienophile.[7a−d] The rigid bicyclo[2.2.2.]octene system in **12** imposes a somewhat different geometrical arrangement on the oxazine ring in this system, in comparison with the favored conformation found for the oxazine ring in the crystal structure of the **6·3** complex (see Figure 3c). As a result, the distance between the two pyridine nitrogens in **12** is calculated to be 9.1 Å, around 1 Å longer than that calculated for **3**.[14] This, in addition to the two Zn−N distances in the transition state complex, approximated to the value as in the **6·3** complex (∼2.2 Å, see above), provides an estimated distance of ∼13.5 Å between the two zinc atoms in the transition state complex, rather than 11.7 Å which was found in the crystal structure for the **6·3** complex (Figure 3c). This implies that the transition state complex experiences maximum strain energy, the two porphyrin moieties being pushed even further apart than in the **6·3** complex.[19] The ability of **6** to change its structure, as manifested in the **6·3** complex (Figure 3c) and even more dramatically expected in the transition state complex, enables **6** to accelerate the reaction of **1** and **2** (see Table 1), although the Zn−Zn distance in the free host **6** (10.576(5) Å, Figure 3a) is much shorter than that in these complexes. The substantial geometrical distortions imposed on **6** (seen in the **6·3** complex and expected in the transition state complex) could account for the modest rate acceleration displayed by **6** compared with trimer **4** (Table 1), in which the Zn−Zn distances across the acetylene linkages are calculated to be 14 Å, similar to that expected in the transition state complex. In support of this idea, trimer **5**, which has three rigid butadiyne linkages, leading to Zn−Zn distances of ∼16 Å and that are much longer than that expected in the transition state complex, is less effective than **4** at accelerating the reaction in Figure 1a.

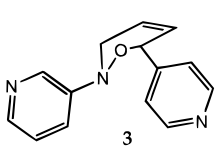

3

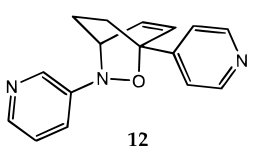

12

As the distance between the two pyridine nitrogens in the transition state is expected to be longer than that in **3** (see above)

(14) (a) The possible geometries of **3** were explored by a Monte-Carlo conformational search and were optimized. The most stable structure for **3** has the same conformation for the oxazine ring and the same type of inversion about the nitrogen atom in this ring, as was found in the **6·3** crystal structure. (b) The computational method used in this work is described in the Experimental and Computational Procedures section.

(15) (a) Anderson, H. L.; Bashall, A.; Henrick, K.; McPartlin, M.; Sanders, J. K. M. *Angew. Chem., Int. Ed. Engl.* **1994**, *33*, 429. (b) Cullen, D. L., Jr.; Meyer, E. F. *Acta Crystallogr.* **1976**, *B32*, 2259. (c) Collins, D. M.; Hoard, J. L. *J. Am. Chem. Soc.* **1970**, *92*, 3761.

(16) Fleischer, E. B.; Shachter, A. M. *Inorg. Chem.* **1991**, *30*, 3763.

(17) (a) As the two porphyrin units in **6** and in the **6·3** complex are qualitatively not offset relative to each other (see Figure 3b,d), this angle is truly describing the degree of leaning toward or away from the cavity of the two porphyrin units in the host. (b) The same is also true for **7** (Figure 4).

(18) Menger, F. M.; Ding, J.; Barragan, V. *J. Org. Chem.* **1998**, *63*, 7578.

(19) (a) This could be seen by examining molecular models. (b) Due to the lack of high-quality Zn···N parameters in force field packages that we know of, we do not present here a calculated structure for the **6·12** complex. Obviously, these type of complexes are too large for high-level molecular orbital calculations with current computational resources available to us.

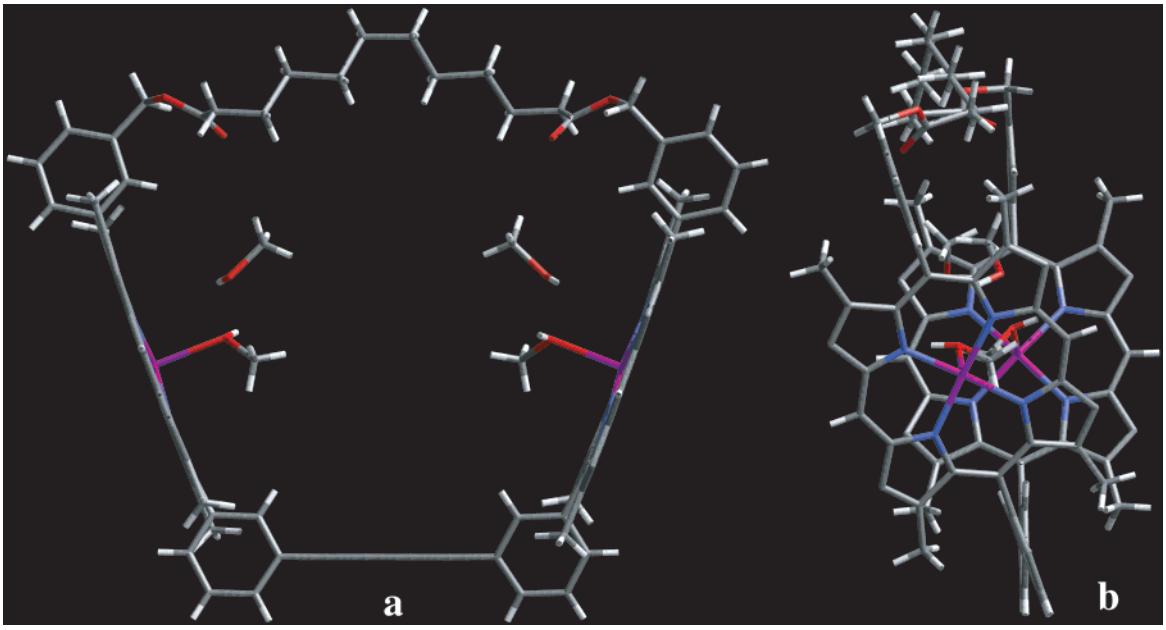

Figure 4. Two views, a and b, of the crystal structure of the cyclic metalloporphyrin **7**. Two MeOH molecules are bound to the Zn atoms in the host, which also contains two additional MeOH molecules that are each hydrogen bonded to the bound methanols. The hexyl side chains (four per porphyrin unit) have been omitted for clarity. Selected key geometrical features for **7**: Zn−Zn distance = 14.625(3) Å; the two Zn atoms lie at a mean distance of 0.14 Å above the N_4 plane [which are nearly coplanar, maximum deviation 0.006 Å (left and right rings)] toward the oxygen atom; relative rotation of porphyrins = 15.1°; Zn−O bond lengths = 2.34(1) Å.

and as the structural changes found on going from the free host **6** to the **6·3** complex are facilitated by the flexible ester linkage, hosts with larger and more flexible linkages, such as $-(CH_2)_{10}-$, as in **7** (see Figure 4), instead of $-(CH_2)_2-$ (as in **6**) should better stabilize the transition state complex and lead to improved acceleration rate. Indeed, host **7** is much more efficient in accelerating the Diels−Alder reaction (in Figure 1a) than **6**, giving 840-fold acceleration rather than 65-fold, respectively (see Table 1). **7** crystallizes from a dichloromethane/hexane/methanol mixture as a methanol-solvate in the monoclinic space group *C*2/*c* (Figure 4). Two hexyl chains (not shown) on each porphyrin unit interpenetrate the cavity of an adjacent dimer, filling the cavity space with four hexyl chains from two adjacent dimers. The other two hexyl chains fill the gaps between porphyrin units of adjacent dimers. The two porphyrin units in **7** are qualitatively planar and have identical structure, as **7** has C_2 symmetry. Two methanol molecules are bound to the zinc atoms within the cavity of **7**. In addition, two methanol molecules are trapped in the cavity of **7** and each is hydrogen bonded to the bound methanol molecules (see Figure 4). The intermolecular O···O distance, 2.55(2) Å, and the O···H distance in each of these pairs of hydrogen bonded MeOH molecules are in the range known for O−H···O type hydrogen bonding.[20,21] The two porphyrin moieties in the crystal structure of **7** are rotated by 15.1° with respect to each other (see Figure 4b) and to a higher degree than in **6** (7.4°, 3.6°, and 6.8°, see above and Figures 2b, 2d, and 3b, respectively). This is probably due to the longer and more flexible $-(CH_2)_{10}-$ linkage in **7** than the $-(CH_2)_2-$ linkage in **6**.

The long and flexible $-(CH_2)_{10}-$ linker in **7** should make it possible for the two porphyrin units in **7** to lean toward or away from the cavity and to a much higher extent than in **6**; indeed, the angles between three meso porphyrin carbons, of which two are connected to the butadiyne linker and one is connected to the ester linker,[17] are 115° for both porphyrin units in **7** (Figure 4a), while in **6** these angles are only 94° (see above and Figure 3a). The long and flexible $-(CH_2)_{10}-$ linker should make it easier for the porphyrin units in **7** to adopt the "right" Zn−Zn distance and leaning angles to accommodate **3** or the transition state for the reaction in Figure 1a.[22] This might be the reason for the higher binding constant found for the **7·3** complex in comparison with the **6·3** complex (see Table 1), although a higher entropic penalty is expected to be paid upon binding of **3** by the more flexible host **7** and for which the Zn−Zn distance is longer by ~3 Å than in the **6·3** complex.[23] Since the N−N distance between the two pyridine nitrogen atoms in the transition state is expected to be longer than in **3** (see above), this effect should be even more dramatic in the transition state to form the Diels−Alder product **3** than in the case of binding **3**. This would account for the significantly higher acceleration rate observed with **7** than with **6** (see Table 1). We are now preparing a series of different but closely related hosts, with a view to exploring the structure−activity relationships kinetically, thermodynamically, and structurally.

By comparison with conventional small molecule crystallography, the *R*-factors associated with the structures described here are rather large. This is hardly surprising: the large unit cell and lack of heavy atoms ensure that the X-ray scattering

(20) For the geometry of hydrogen bonding see: (a) Allen, F. H.; Motherwell, W. D. S.; Raithby, P. R.; Shields, G. P.; Taylor, R. *New J. Chem.* **1999**, *23*, 25. (b) Jeffrey, G. A.; Saenger, W. *Hydrogen Bonding in Biological Structures*; Springer-Verlag: Berlin, 1991.

(21) As the precision in the location of hydrogen atoms is less than that for oxygen atoms, we present the O···O distances.

(22) Unfortunately, many attempts to obtain single crystals suitable for X-ray crystallography for the **7·3** complex were not successful.

(23) Obviously, entropic factors due to different desolvation processes for binding **3** to hosts **6** vs **7** could also partially contribute to the binding constants measured between these hosts and the Diels−Alder product **3**: It is likely that in solution host **7** would contain more solvent molecules in its cavity than the smaller host **6**. Therefore, this could lead to a different entropic gain due to solvent release upon binding of **3** in the cavity of **6** vs **7** (see text above). However, this does not have to be always the case, as having more solvent molecules in a larger cavity does not necessarily ensure that more solvent molecules will be displaced by the ligand. The desolvation process upon binding of ligands inside the cavity of host molecules is a complex phenomenon and, therefore, only some possible qualitative aspects of this problem are discussed here.

power of the crystals will be very low,[24] while the four solubilizing hexyl chains per porphyrin unit tend to be disordered; furthermore, solvent molecules are often included within and between molecules in the lattice. In general, therefore, we have needed recourse to synchrotron sources of X-rays. It is important to note that although the large *R*-factors associated with this kind of system inevitably limit the precision with which one can determine bond lengths and angles, they do not detract from our ability to draw conclusions about intermolecular interactions or large scale molecular distortions.

Conclusions

In this study we have demonstrated, for the first time for synthetic receptors, a detailed structural analysis of the geometrical changes imposed on an accelerating agent on binding of a Diels−Alder product. We have confirmed the importance of host flexibility, for acceleration of the hetero-Diels−Alder within the cavity of a cyclic metalloporphyrin receptor. This opens the possibility of exploring in detail the influence of host geometry changes on acceleration rates and will direct us in the design of new and better accelerating metalloporphyrin receptors. The absence of solvent molecules from the host−guest **6·3** complex (Figure 3c,d), in contrast to the solvated crystal structures of the free host **6** (Figures 2 and 3a,b), implies that solvent stabilization is not as significant for the host-accelerated reaction as in the control (host free) reaction, a conclusion that had previously been reached from kinetic and binding results.[5]

Experimental and Computational Procedures

General. ^{1}H NMR spectra (250 MHz) was recorded on Bruker AC-250 spectrometers. ^{13}C NMR spectra were obtained on a Bruker AC-250 operating at 62.5 MHz. All NMR measurements were carried out at room temperature in deuteriochloroform. Fast atom bombardment mass spectra (FAB MS) were recorded on a Kratos MS-50 mass spectrometer. MALDI-TOF mass spectra were recorded on a Kratos Analytical Ltd., Kompact MALDI IV mass spectrometer. A nitrogen laser (337 nm, 85 kW peak laser power, 3 ns pulse width) was used to desorb the sample ions, and the instrument was operated in linear time-of-flight mode with an accelerating potential of 20 kV. Results from 50 laser shots were signal averaged to give one spectrum. An aliquot (1 μL) of a saturated solution of the matrix (sinapinic acid) was deposited on the sample plate surface. Before the matrix completely dried, a small volume (1 μL) of analytes (dissolved in dichloromethane/chloroform at 1 mg/mL) was layered on the top of the matrix and allowed to air-dry.

Deprotected 10: Monomer **9** (232 mg, 0.223 mmol, 2.1 equiv), DMAP (48 mg, 0.39 mmol), and triethylamine (33 μL, 0.23 mmol) were added to a stirring solution of succinyl dichloride (12 μL, 0.106 mmol, 1 equiv) in tetrahydrofuran (20 mL, freshly distilled over $LiAlH_4$/CaH_2) at 0 °C. After 2 h the mixture was allowed to warm to room temperature after which stirring was continued for a further 12 h. The solvent was removed by evaporation to give a red solid before redissolving in dichloromethane (100 mL). The mixture was washed with saturated sodium bicarbonate solution (3 × 100 mL) and water (3 × 100 mL), dried over $MgSO_4$, and evaporated to dryness. The product was purified by column chromatography on silica, eluting with hexane/ethyl acetate (3:1 v/v), and the solvent was removed by evaporation to give a red solid. This product was redissolved in dichloromethane (150 mL) and excess TBAF added (300 μL of a 1.1 M solution in tetrahydrofuran, 0.33 mmol). The mixture was stirred under a drying tube for 10 min, after which no starting material could be detected by TLC (3:1 v/v ethyl acetate/hexane). Excess calcium chloride was added to quench any remaining TBAF (4−5 spatula tips) and the mixture washed with water (2 × 100 mL), dried ($MgSO_4$), filtered, and evaporated to give 118 mg of the deprotected **10** (52%). ^{1}H NMR (250 MHz, $CDCl_3$) δ 0.91−1.02 (24H, m, hexyl Me), 1.30−1.54 (32H, s, hexyl CH_2), 1.74 (16H, m, hexyl CH_2), 2.09−2.55 (16H, m, hexyl CH_2 + 24H, ring Me + 4H, CH_2 cap), 3.19 (2H, s, C≡C−H), 3.70−4.26 (16H, s, CH_2-Por), 5.37, 5.38 (4H, 2 × s, benzyl CH_2), 7.56−8.33 (16H, m, aryl-H), 9.93, 10.08, 10.21 (4H, 3 × s, meso-H); ^{13}C NMR (62.5 MHz, $CDCl_3$, APT) δ 13.94, 14.67, 15.15, 15.62 (Me), 19.72, 20.58, 22.77, 23.96, 26.73, 29.32, 30.08, 31.99, 33.35 (CH_2), 66.78 (CH_2O-aryl), 83.94 (C≡*C*−Ar), 97.49 (meso), 117.80, 118.54, 121.37, 134.92, 137.60, 137.71, 141.50, 143.34, 143.66, 143.92, 144.11, 146.18, 146.29, 147.41 (quaternary pyrrole and aryl carbons), 127.57, 127.58, 127.59, 127.61, 131.82, 132.81, 133.09, 133.74, 136.77 (aryl-H), 172.09 (ester C═O); FABMS ($C_{130}H_{162}N_8O_4Si_2Zn_2$) calcd 2027.130, found 2027.5.

Host 6: The deprotected **10** (118 mg, 0.058 mmol) was dissolved in dry dichoromethane (340 mL) and subjected to Glaser-Hay coupling cyclization conditions; freshly prepared copper(I) chloride (402 mg, 4.06 mmol, 70 equiv) and TMEDA (0.62 mL, 4.06 mmol, 70 equiv) were added and the solution stirred for 15 h at room temperature under a drying tube. The mixture was washed with water (6 × 200 mL), the organics were dried ($MgSO_4$) and filtered, and the solvent was removed by evaporation to give a red solid. The cyclic product was purified by chromatography on silica, eluting with hexane/ethyl acetate (4:1 v/v), and recrystallized from chloroform/methanol (88 mg, 75%). ^{1}H NMR (250 MHz, $CDCl_3$) δ 0.76−0.81 (24H, m, hexyl Me), 1.14−1.39 (32H, m, hexyl CH_2), 1.51−1.59 (16H, m, hexyl CH_2), 1.95 (16H, m, hexyl CH_2), 2.20, 2.26 (24H, 2 × s, ring Me), 2.29 (4H, s, CH_2 cap), 3.71 (16H, m, CH_2-Por), 5.21 (4H, s, benzyl CH_2), 7.42 (2H, s, aryl-H2), 7.45 (2H, s, aryl-H2′), 7.54−7.72 (8H, m, aryl-H), 8.16 (2H, d, J = 6.8 Hz, aryl-H), 8.35 (2H, d, J = 6.8 Hz, aryl-H), 9.83 (4H, s, meso-H); ^{13}C NMR (62.5 MHz, $CDCl_3$, APT) δ 13.90, 15.07, 15.48 (Me), 22.57, 26.53, 28.27, 29.85, 31.78, 33.14 (hexyl CH_2), 66.36 (benzyl CH_2), 74.39, 78.08 (C≡C), 97.03 (meso), 112.63, 116.74, 119.81, 120.05, 120.78, 134.71, 137.02, 137.33, 143.10, 143.28, 144.44, 146.02, 147.22, 147.30 (quaternary pyrrole and aryl carbons), 126.99, 127.11, 127.38, 129.27, 132.43, 132.85, 133.13, 139.74 (aryl-H), 172.34 (ester C═O); MALDI-TOF ($C_{130}H_{160}N_8O_4Zn_2$) calcd 2025.114, found 2025.1.

Host 7: The preparation and spectroscopic data for **7** are described elsewhere.[10]

Molecular Modeling. Molecular modeling was carried out on a Silicon Graphics Indy workstation using CERIUS^2 version 3.0 (BIOSYM/Molecular Simulations) with the UNIVERSAL 1.02 force field.[25] Atom and bond parameters were taken directly from the program database. In comparison with the **6·3** crystal structure, the program severely underestimates the pyramidal angle around the nitrogen atom in the oxazine ring. Therefore, we fixed that pyramidal angle to the value found in the **6·3** crystal structure. The MM2 and MM3 force fields calculate a similar degree of pyramidalization about the oxazine nitrogen for a model of **3** (in which the pyridine rings were replaced with Me substituents) as in the **6·3** complex. However, the MM2 and MM3 force fields lack the parameters for a pyridine substituted **3** and therefore were not used. Fixing the pyramidal angle around the oxazine nitrogen is further justified, as ab initio molecular orbital calculations (at the HF/6-31G* level) show a nearly identical pyramidal angle about the nitrogen in *N*-Me-oxazine (used as a model for **3**) to that found in the **6·3** crystal structure.

Single-Crystal Structure Determinations. After much effort, only very small crystals of **6** (MeOH) solvate, **6·3**, and **7** (MeOH) solvate could be grown. These proved to be only weakly diffracting. To determine these structures it was necessary to exploit the high intensity of a synchrotron radiation source. Data were collected at the Daresbury SRS (UK), Station 9.8, using a Bruker AXS Smart CCD area-detector diffractometer, in narrow frame mode.[26,27] Intensities were integrated[28]

(24) Harding, M. M. *J. Synchrotron Radiat.* **1996**, *3* (No. Pt6), 250.

(25) Rappé, A. K.; Casewit, C. J.; Colwell, K. S.; Goddard, W. A., III; Skiff, W. M. *J. Am. Chem. Soc.* **1992**, *114*, 10024.

(26) Cernik, R. J.; Clegg, W.; Catlow, C. R. A.; Bushnell-Wye, G.; Flaherty, J. V.; Greaves, G. N.; Hamichi, M.; Borrows, I. D.; Taylor, D. J.; Teat, S. J. *J. Synchrotron Radiat.* **1997**, *4*, 279.

(27) Clegg, W.; Elsegood, M. R. J.; Teat, S. J.; Redshaw C.; Gibson, V. C. *J. Chem. Soc., Dalton Trans.* **1998**, 3037.

(28) SMART (control) and SAINT (integration) software, version 4; Bruker AXS Inc.: Madison, WI 1994.

from several series of exposures. For **6** (which was grown from a dichloromethane/hexane/methanol mixture, Figure 2) each exposure covered 0.5° in ω, with an exposure time of 2 s, and the total data set was more than a hemisphere. For **6·3** each exposure covered 0.6° in ω, with an exposure time of 1 s, and the total data set was more than a hemisphere. For **7** each exposure covered 0.3° in ω, with an exposure time of 10 s, and the total data set was more than a hemisphere. Data were corrected for absorption and incident beam decay.[29] The unit cell parameters were refined using LSCELL.[30] Crystals grown for **6** (toluene/MeOH) solvate were of a sufficient quality to use for structure determination with a conventional laboratory X-ray source. Measurements were made using a Rigaku R-Axis IIc imaging plate system. Integration and data reduction was performed within the R-AXIS PROCESS[31] software.

Even using a synchrotron radiation source, these crystals were found to be weakly diffracting because of extensive disorder of the *n*-hexyl chains. This resulted in relatively high *R*1 values. The carbon atoms in these disordered groups were refined with isotropic temperature factors and restrained to give chains with a reasonable geometry.

Crystal data for 6 (MeOH solvate, Figure 2): $C_{136}H_{180}N_8O_{10}Zn_2$, M_r 2217.62, red crystals from a dichloromethane/hexane/methanol mixture (crystal dimensions 0.28 × 0.16 × 0.16 mm^3); monoclinic, space group $P2_1/c$(14), a = 29.750(4) Å, b = 29.301(4) Å, c = 29.914(4) Å β = 90.670(10)°, V = 26074(6) Å^3, Z = 8, ρ_{calc} = 1.130 Mg m^{-3}, μ = 0.426 mm^{-1}; θ_{max} = 22.56° (Mo Kα), λ = 0.6887 Å, T = 150(2) K; 81486 measured reflections of which 31773 were independent [R(int) = 0.1044]; final residuals (31773 included reflections, 1278 parameters) $R1[I > 2\sigma(I)]$ = 0.1454, $wR2$ = 0.3291, S = 1.077 ($w = 1/[\sigma^2F_o^2 + (0.1008P)^2 + 439.7665P]$, where $P = (F_o^2 + 2F_c^2)/3$). Hydrogen atoms were fixed geometrically, riding on the relevant atom and refined with isotropic temperature factors. The largest peak and hole in the difference map are 1.61 and −1.008 eÅ^{-3}, respectively. The structure was solved by direct methods using SIR-92[32] and refined with SHELXL-97.[33]

Crystal data for 6 (toluene/MeOH solvate, Figure 3a,b): $C_{146}H_{180}N_8O_6Zn_2$, M_r = 2273.72, red crystals from a toluene/methanol mixture (crystal dimensions: 0.20 × 0.20 × 0.20 mm^3); orthorhombic, space group *Pbca* (no. 61) a = 30.686(10) Å, b = 30.124(10) Å, c = 28.941(10) Å, V = 26753(16) Å^3, Z = 8, ρ_{calc} = 1.129 Mg m^{-3}, μ = 0.415 mm^{-1}; $2\theta_{max}$ = 41.46°, λ = 0.71069 Å, T = 180(2) K, F(000) = 9760; 23547 measured reflections of which 12688 were independent [$R_{(int)}$ = 0.097]; final residuals (12688 included reflections, 508 parameters) $R1[I > 2\sigma(I)]$ = 0.1626, $wR2$ = 0.4010, S = 1.155 ($w = 1/[\sigma^2F_o^2 + (0.2P)^2]$, where $P = (F_o^2 + 2F_c^2)/3$)). Hydrogen atoms were fixed geometrically, riding on the relevant heavy atom and refined with isotropic temperature factors. The largest peak and hole in the final difference map are 1.160 and −0.706 eÅ^{-3}, respectively. The structure was solved by direct methods using SIR-92[32] and refined with SHELXL-97.[33]

Crystal data for the 6·3 complex: $C_{144}H_{169}N_{11}O_5Zn_2$, M_r = 2264.64, red microcrystals from a dichloromethane/hexane/methanol mixture (crystal dimension 0.20 × 0.20 × 0.02 mm^3); monoclinic, space group $P2_1/n$ (no. 14), a = 16.174(2) Å, b = 29.754(5) Å, c = 28.970(4) Å, β = 102.63(10)°, V = 13604(3) Å^3, Z = 4, ρ_{calc} = 1.106 Mg m^{-3}, μ = 0.408 mm^{-1}; $2\theta_{max}$ = 40.00°, λ = 0.6919 Å (synchrotron), T = 150(2) K, F(000) = 4840; 31413 measured reflections of which 12891 were independent [$R_{(int)}$ = 0.1197]; final residuals (12891 included reflections, 574 parameters) $R1[I > 2\sigma(I)]$ = 0.1899, $wR2$ = 0.4217, S = 1.407 ($w = 1/[\sigma^2F_o^2 + (0.2P)^2]$, where $P = (F_o^2 + 2F_c^2)/3$). Hydrogen atoms were fixed geometrically, riding on the relevant heavy atom and refined with isotropic temperature factors. The largest peak and hole in the final difference map are 1.064 and −0.834 eÅ^{-3}, respectively. The structure was solved by direct methods using SIR-92[32] and refined with SHELXL-97.[33]

Crystal data for 7 (MeOH solvate, Figure 4): $C_{142}H_{188}N_8O_8Zn_2$, M_r = 2265.74, red crystals from a dichloromethane/hexane/methanol mixture (crystal dimensions 0.12 × 0.10 × 0.03 mm^3); monoclinic, space group $C2/c$ (no. 15) a = 8.038(1) Å, b = 32.731(4) Å, c = 47.780(6) Å, β = 91.410(10)°, V = 12567(3) Å^3, Z = 4, ρ_{calc} = 1.198 Mg m^{-3}, μ = 0.442 mm^{-1}; θ_{max} = 22.50° (Mo Kα), λ = 0.6890 Å, T = 150(2) K; 27697 measured reflections of which 8971 were independent [R(int) = 0.0852]; final residuals (8971included reflections, 655 parameters) $R1[I > 2\sigma(I)]$ = 0.1469, $wR2$ = 0.3448, S = 1.153 ($w = 1/[\sigma^2F_o^2 + (0.1342P)^2 + 177.0312P]$, where $P = (F_o^2 + 2F_c^2)/3$). Hydrogen atoms were fixed geometrically, riding on the relevant atom and refined with isotropic temperature factors. The largest peak and hole in the difference map are 1.141and −0.708 eÅ^{-3}, respectively. The structure was solved by direct methods using SIR-92[32] and refined with SHELXL-97.[33]

Acknowledgment. This work was supported by the British Council, Israel Academy and Ministry of Science, and B′nai B′rith.

Supporting Information Available: Tables of crystal data, structure solution and refinement, atomic coordinates, bond lengths and angles, and anisotropic thermal parameters for solvated **6** and **7** and for the **6·3** complex (PDF). This material is available free of charge via the Internet at http://pubs.acs.org.

JA9922227

(29) G. M. Sheldrick, SADABS, program for scaling and correction of area detector data; University of Göttingen, 1997 (based on the method of Blessing: Blessing, R. H. *Acta Crystallogr. Sect A* **1995**, *51*, 33).

(30) Clegg, W.; LSCELL, program for refinement of cell parameters from SMART data; University of Newcastle upon Tyne, 1995.

(31) For R-AXIS PROCESS: Molecular Structure Corporation, 1995. PROCESS Version 3.2. MSC, 3200 Research Forest Drive, The Woodlands, TX 77381, 1997.

(32) Altomare, A.; Cascarano, G.; Giacavazzo, C.; Guagliardi, A.; Burla, M. C.; Polidori, G.; Camalli, M. C. *J. Appl. Crystallogr.* **1994**, *27*, 435.

(33) G. M. Sheldrick, 1997; SHELXL97, Program for the Refinement of Crystal Structures; University of Göttingen, Germany.